

Self-Assembly of Perovskite Nanoplates in Colloidal Suspensions

*¹Raphael F. Moral, ²Antônio A. Malfatti-Gasperini, ³Luiz G. Bonato, ³Brener R. C. Vale,
¹André Fonseca, ³Lazaro A. Padilha, ⁴Cristiano L. P. Oliveira, ¹Ana F. Nogueira**

¹Instituto de Química – Universidade Estadual de Campinas (UNICAMP), Campinas – SP, Brasil

²Brazilian Center for Research in Energy and Materials (CNPEM), Campinas – SP, Brazil

³Instituto de Física Gleb Wataghin – Universidade Estadual de Campinas (UNICAMP), Campinas – SP, Brasil

⁴Institute of Physics – University of São Paulo (IFUSP), São Paulo – SP, Brazil

Email: anafla@unicamp.br

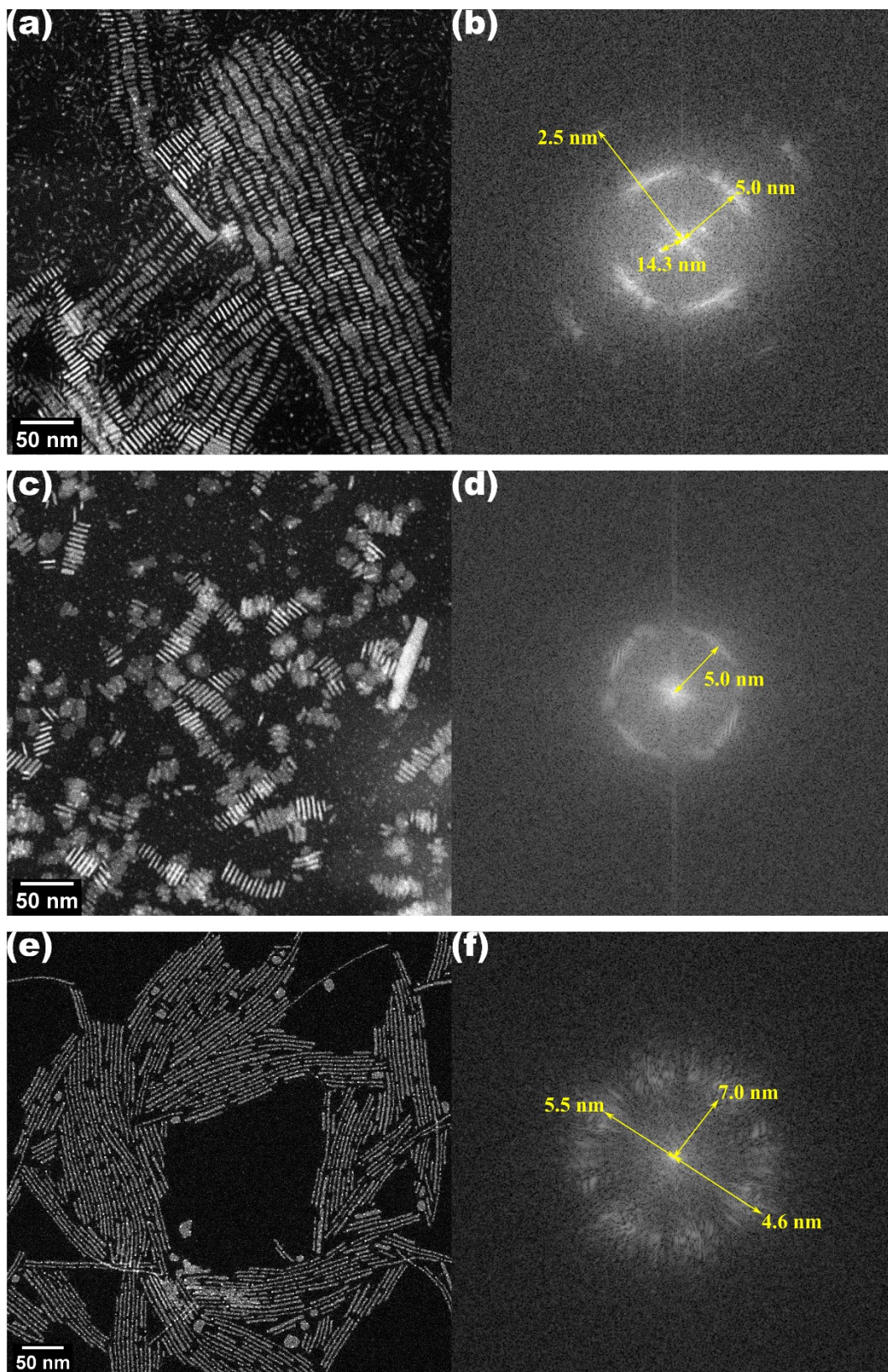


Figure S1. HAADF-STEM and their respective FFTs images of **a-b)** Sample Br-170, **c-d)** Sample I-110, and **e-f)** Sample Br-110.

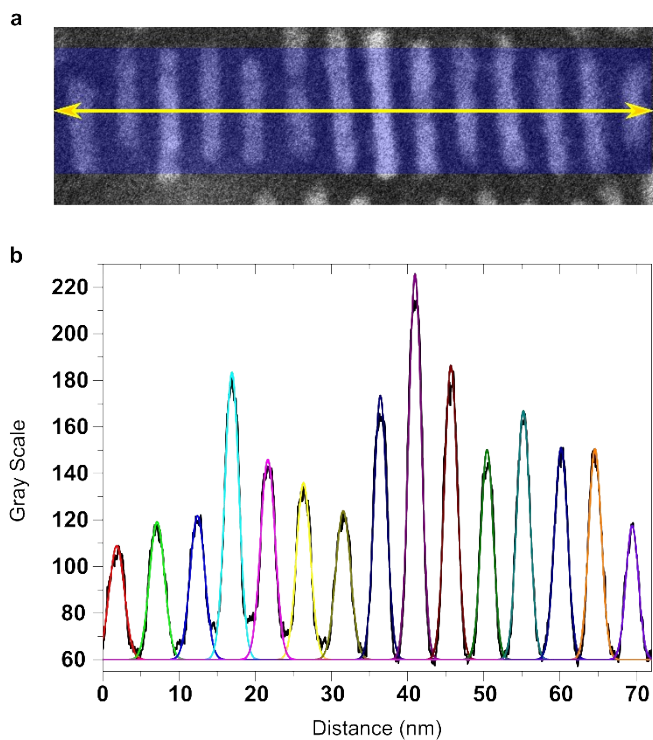


Figure S2. a) An example of a segment of nanoplates to extract the intensity profile for thickness measurements and b) an example of the intensity profile of a segment of nanoplates with gaussian functions fit to each peak; the thickness of the nanoplates were taken as the FWHM of the gaussian functions.

Table S1. Summary of the parameters and estimative of the thickness of the particles extracted from the intensity profiles of the samples as shown in **Figure S2**

| Sample | N Sampling | Estimate Thickness (nm) | Number of Layers (approximated) | Interparticle Distance (nm) | Organic Bilayer Length (nm) |
|----------------|------------|-------------------------|---------------------------------|-----------------------------|-----------------------------|
| Br-110 | 86 | 2.52 ± 0.45 | 4 | 5.5 | 2.98 |
| Br-170 | 84 | 2.28 ± 0.38 | 4 | 5.0 | 2.72 |
| I-110 | 110 | 2.36 ± 0.41 | 4 | 5.0 | 2.64 |
| Average | | | | | 2.78 ± 0.18 |

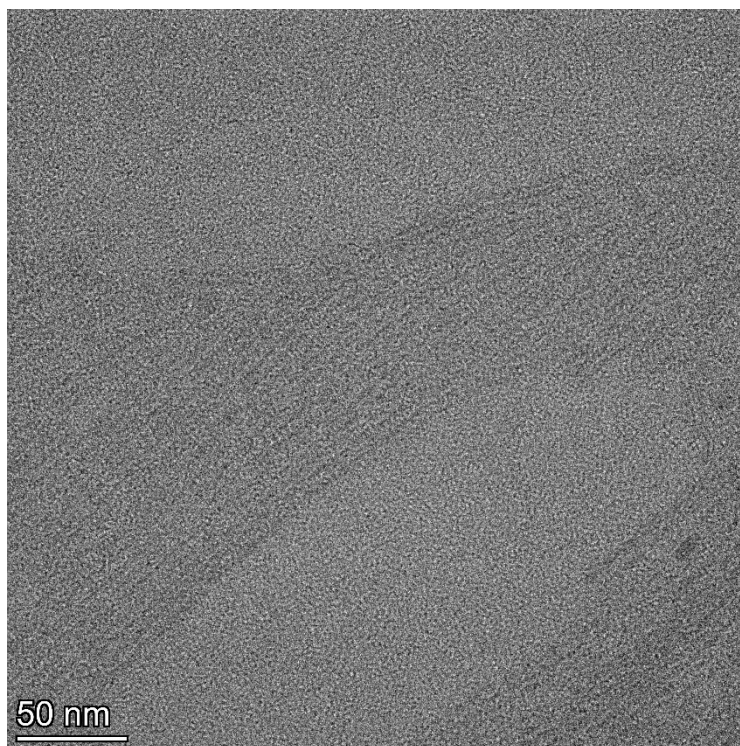


Figure S3. TEM image of sample Br-110 presenting a low contrast of the nanowires. The low contrast suggests thin NWs, consistent to the $n = 2$ thickness observed in the absorption spectrum.

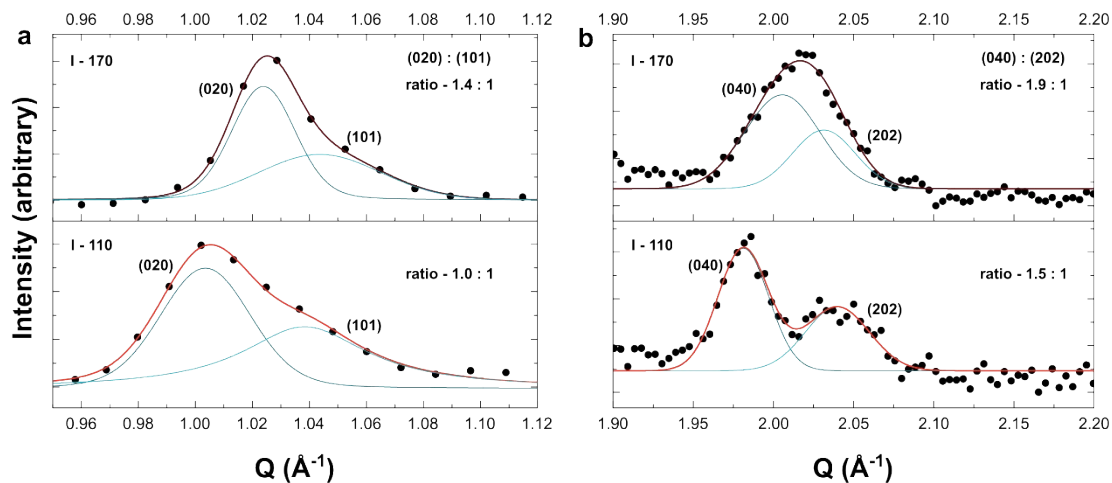


Figure S4. **a**) Diffractions with Miller indexes (020) and (101) extracted from the SAXS curves from **Figure 3** of the main text: top = I-170 and bottom = I-110; **b**) Diffractions with Miller indexes (040) and (202) extracted from the WAXS curves from **Figure 2e** of the main text: top = I-170 and bottom = I-110. The blue curves are the fits to the individual peaks, and the red curves are the cumulative fit curves. The ratio (0k0):(h0l) diminishes as the thickness of the nanoplates decreases from sample I-170 to sample I-110. This occurs because the diffractions from the {0k0} planes are highly affected by the thickness of the nanoplates (position and relative intensity), while the diffractions from the {h0l} planes are nearly not affected. This suggests that the thickness of the nanoplates is in the [0k0] direction.

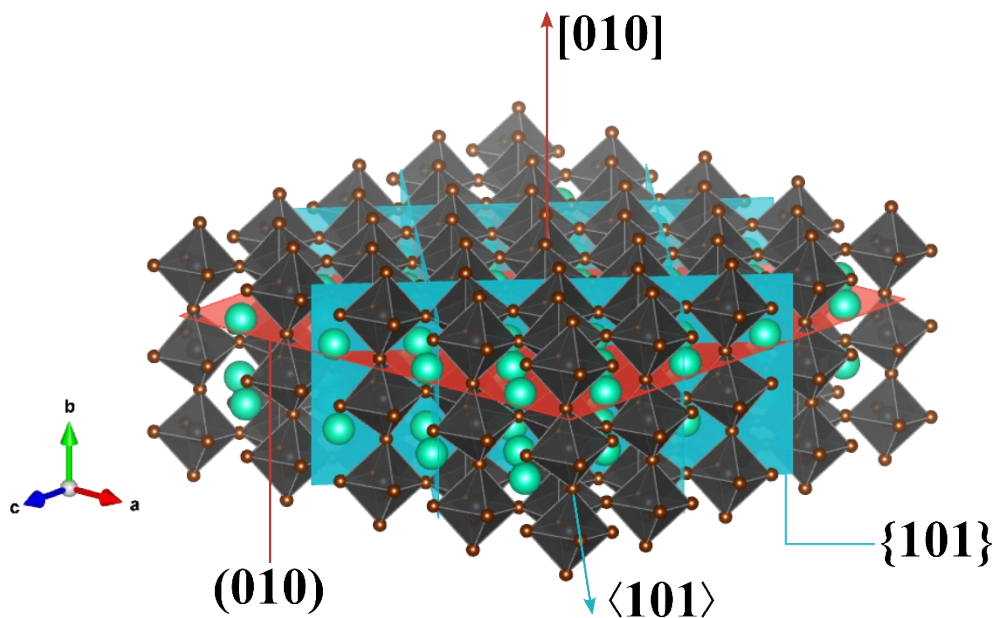


Figure S5. Schematic representation of a $n = 3$ CsPbBr₃ nanoplate with the generic directions $\langle 101 \rangle$ and direction $[010]$ and their respective perpendicular planes.

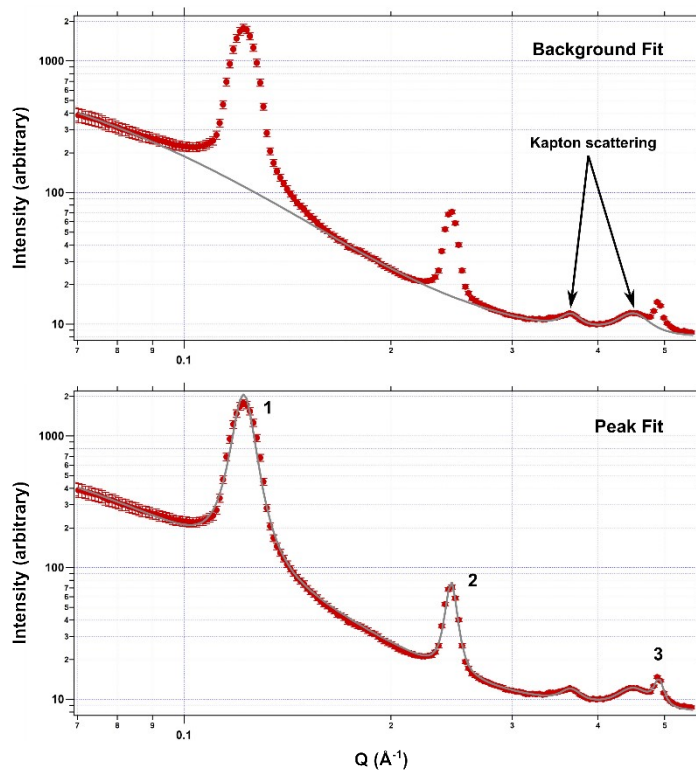


Figure S6. Example of fit to the dry samples of **Figure 3** in the main text: the upper panel shows the background fit with 3 different spherical size populations with no physical meaning, and the bottom panel shows the fit of the diffractions with Lorentzian functions.

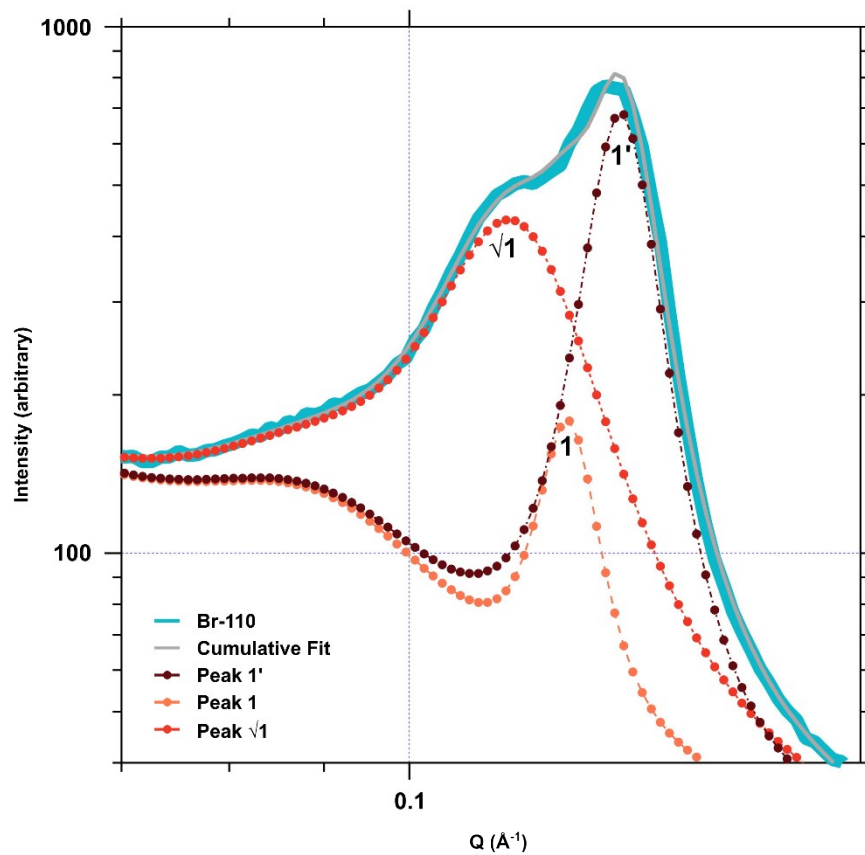


Figure S7. Deconvolution of the main diffractions of the Br-110 dry sample showing 3 distinct diffraction peaks, each assigned to a crystallographic phase.

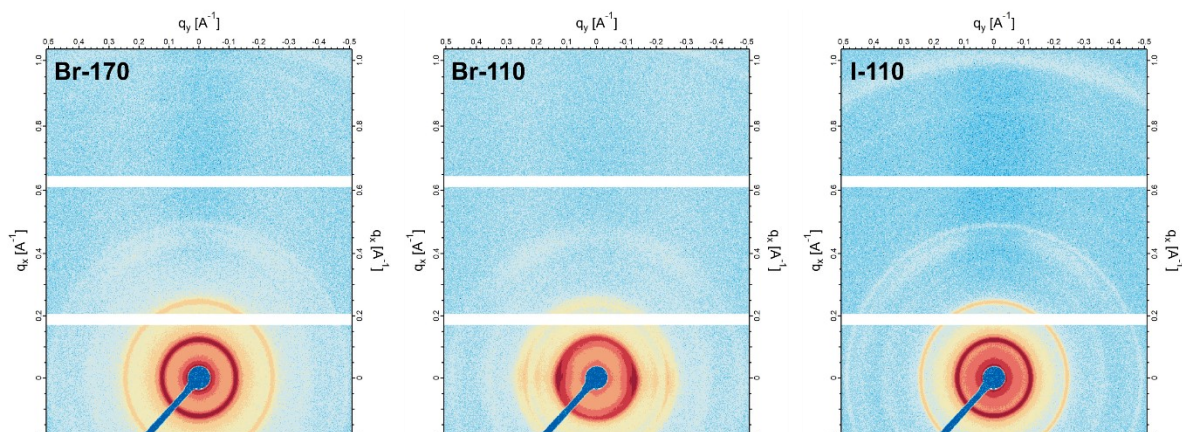


Figure S8. 2D scattering images of the solid samples of **Figure 3** in the main text; the scattering pattern of sample Br-110 shows a preferential orientation along the Q_y axis due to a gravitational action on the nanowires.

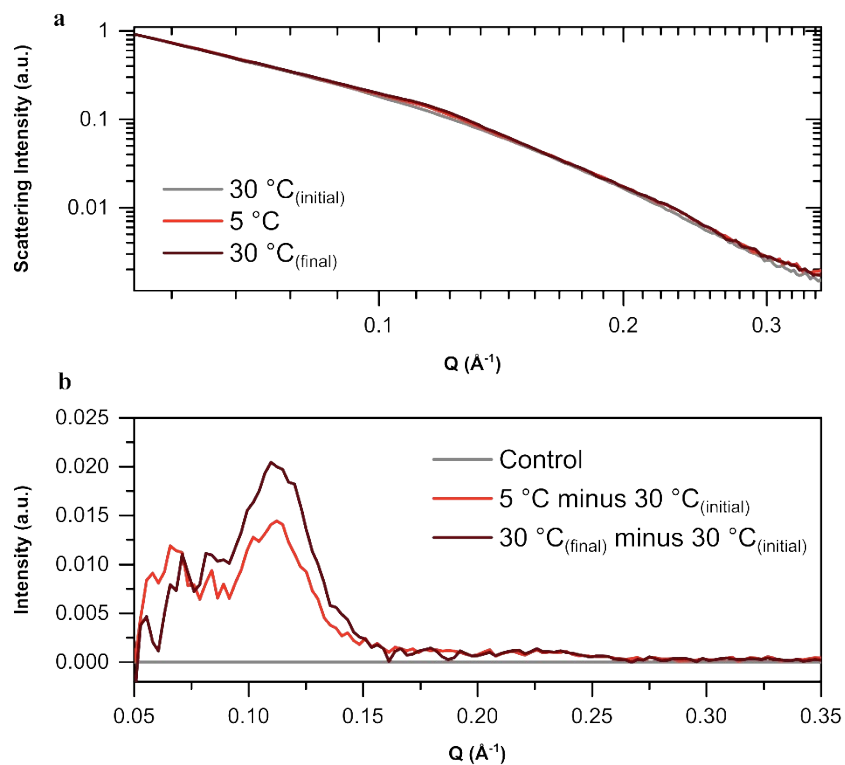


Figure S9. Aggregation induced by temperature in sample I-110 in hexane (80 mg/mL). **a)** overlap of three SAXS curves from **Figure 4c** in the main text: 30 °C_(initial), 5 °C, and 30 °C_(final); **b)** subtraction of the curves in **(a)** evidencing aggregation by the appearance of scattering peaks as the temperature of the sample is decreased.

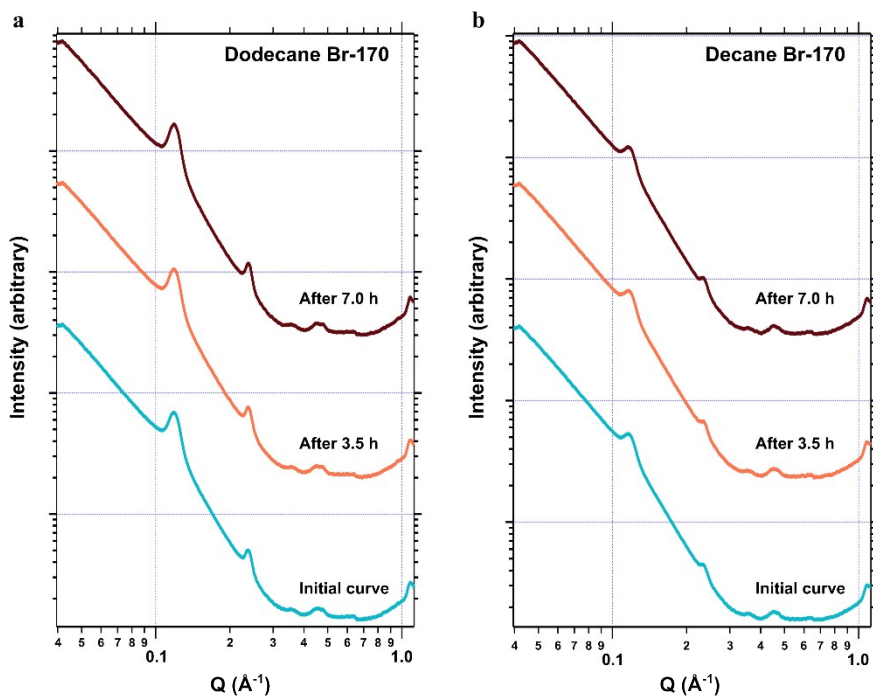


Figure S10. SAXS curves of **a)** a dodecane suspension with a concentration of 80 mg/mL of sample Br-170 measured along seven hours; and **b)** its analogue suspension in decane.

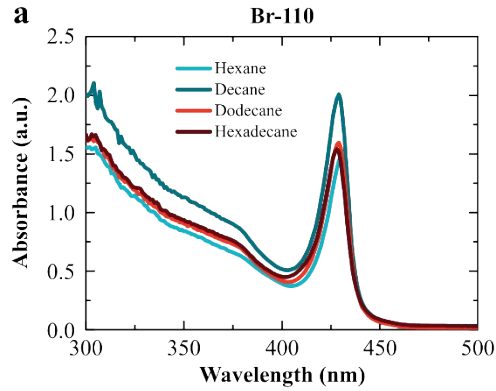


Figure S11. Absorption spectra of each suspension of CsPbBr₃ NWs synthesized at 110 °C (Br-110 – 0.2mg/mL) in the four different solvents used to carry out SAXS experiments. Peak position and general absorption onset are the same in all cases, and no evidence of minority $n = 3$ NWs' population can be seen in any spectra.

Figure S12. – FRET efficiency curves as a function of the distance between donor and acceptor species with both $1/r^6$ and $1/r^4$ dependencies ($k = 1$): **a)** Br-110 $n = 2$ to $n = 3$ donor-acceptor system; **b)** Br-170 $n = 3$ to $n = 3$ donor-acceptor system (homo-FRET); and **c)** I-110 $n = 3$ to $n = 3$ donor-acceptor system (homo-FRET). The distance found in SAXS experiments for the PNPIs stacks are all lower than the R_0 calculated for their donor-acceptor systems.

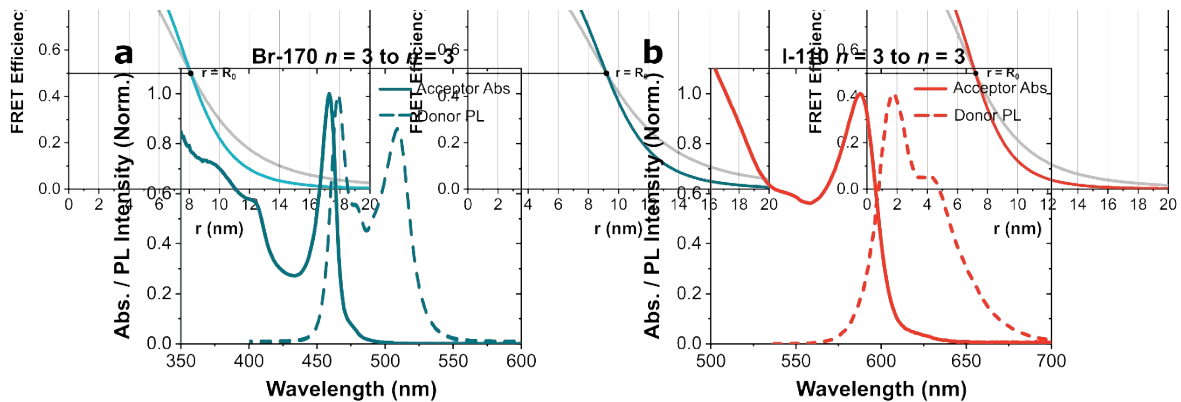


Figure S13. Overlap between absorption and emission spectra of donor and acceptor systems in **a)** Br-170 (homo-FRET) and **b)** I-110 (homo-FRET). There is considerable overlap even between PNPIs with the same thickness ($n = 3$).

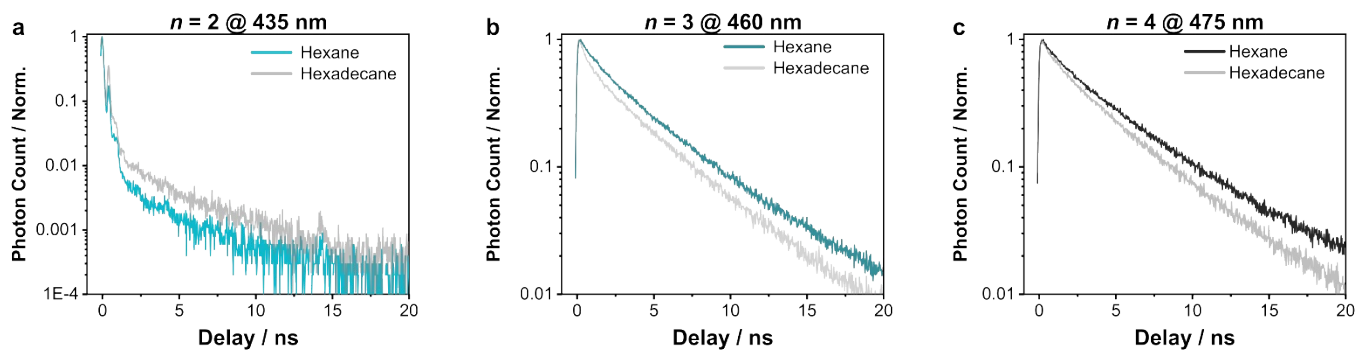


Figure S14. **a)** Time-resolved PL decays measured at 435 nm ($n = 2$ emission) of two Br-170 suspensions in hexane and hexadecane; **b)** time-resolved PL decays measured at 460 nm ($n = 3$ emission) of two Br-170 suspensions in hexane and hexadecane; **c)** time-resolved PL decays measured at 475 nm ($\sim n = 4$ emission) of two Br-170 suspensions in hexane and hexadecane. The decay curves do not show an obvious behavior in terms of energy transfer. This could be associated to the energy cascade between the $n = 3$ PNPIs and other subpopulations such as $n \geq 4$, as can be visualized in **Figure S13a**.

Supplementary Text

Absorption Cross-section measurements

Absorption cross-section measurements were performed using the TCSPC setup as reported earlier by Nagamine et al.¹ The probability of having N excitons per particle is given by the Poisson statistic, **Eq. S1**.

$$P(n) = \frac{\langle N \rangle^n \cdot e^{-\langle N \rangle}}{n!} \quad \text{Eq. S1}$$
$$\langle N \rangle = \sigma_{3.1 \text{ eV}} j$$

Where $\sigma_{3.1 \text{ eV}}$ is the absorption cross-section of the material at 3.1 eV, j is the density of photons per pulse per area. The product between $\sigma_{3.1 \text{ eV}}$ and j gives the average excitons occupancy per particle. Since the band-edge of perovskite is 2-fold degenerate, the PNPLs will be populated by up to two excitons. The particles that have absorbed only one photon contribute only once to the signal, while all others that have absorbed more than one will contribute twice. For long time delay (> 2 ns), all biexcitons will have already decayed via Auger recombination, and the NCs will be occupied with only one exciton per particle. In this way, the PL intensity at 5 ns was modeled by **Eq. S2**:

$$PL = A[1 - P(0)] = A(1 - e^{-\langle N \rangle}) \quad \text{Eq. S2}$$

The laser beam waist was measured using the Knife-edge method.² In **Figure S15a** we show the PL decay of CsPbBr₃ PNPLs with different pump fluences. Then, we integrated the signal at 5 ns for the different fluences and plotted the PL intensity versus the photon fluences, **Figure S15b**. By fitting the experimental data with the **Eq. S2**, we found an absorption cross-section of $6.8 \pm 0.5 \times 10^{-15} \text{ cm}^2$ at 3.1 eV. This value is in good agreement with other data from the literature for CsPbBr₃ PNPLs with $n = 3$.³⁻⁵ From the absorption cross-section value, we calculated the absorption coefficient (ϵ) through **Eq. S3**, to be equal to $1.8 \times 10^6 \text{ L mol}^{-1} \text{ cm}^{-1}$.

$$\epsilon = \frac{\sigma_{3.1 \text{ eV}} N_A}{2.3 * 1000} \quad \text{Eq. S3}$$

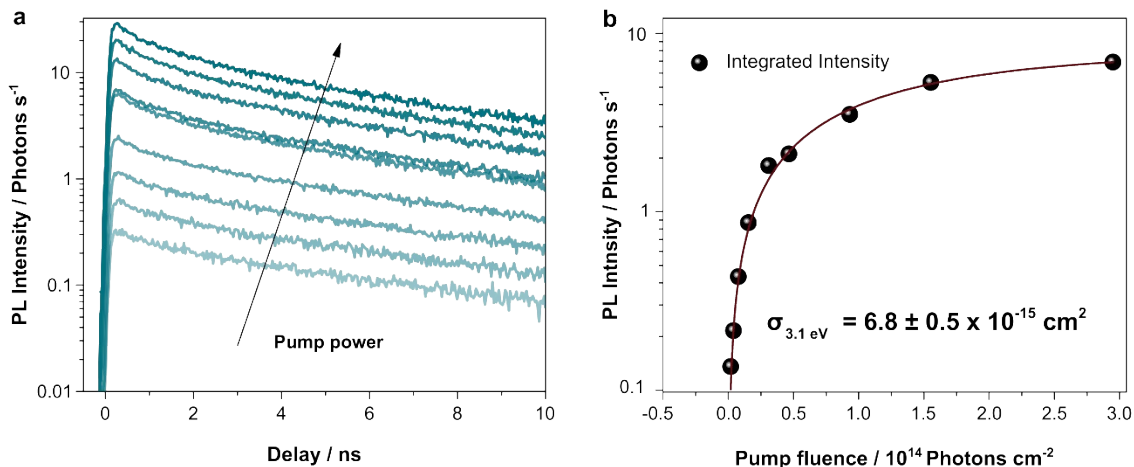


Figure S15. **a)** PL decay curves of CsPbBr₃ PNPIs at different pump fluences probed at 511 nm. **b)** PL intensity measured at 5 ns from the PL decay curves of **(a)** versus pump fluence. Pump wavelength was set at 400 nm.

For CsPbI₃ $n = 3$, we used a similar procedure, and we found an absorption cross section of $3.0 \times 10^{-14} \text{ cm}^2$ (**Figure S16**).

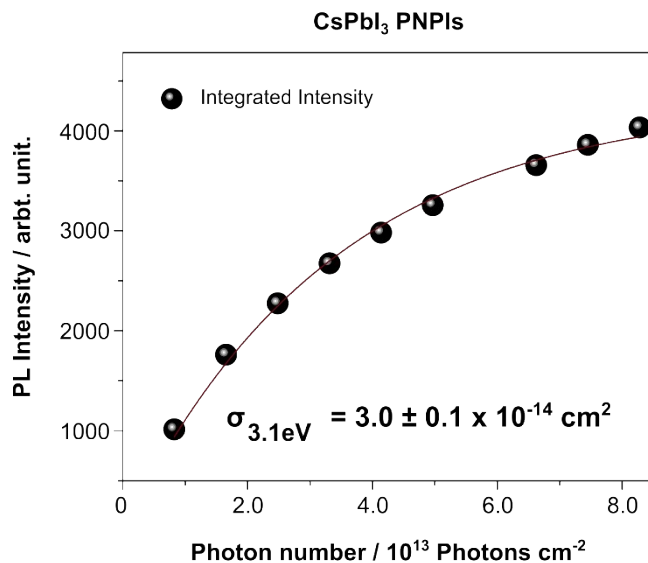


Figure S16. PL intensity measured for CsPbI₃ versus pump fluence. Pump wavelength was set at 400 nm.

Supplementary References

1. Nagamine, G. *et al.* Two-Photon Absorption and Two-Photon Induced Gain in Perovskite Quantum Dots. *J. Phys. Chem. Lett.* **9**, 3478–3484 (2018).
2. Nemoto, S. Determination of Waist Parameters of a Gaussian Beam. *Appl. Opt.* **25**, 3859–3863 (1986).
3. Vale, B. R. C. *et al.* Exciton, Biexciton, and Hot Exciton Dynamics in CsPbBr₃ Colloidal Nanoplatelets. *J. Phys. Chem. Lett.* **11**, 387–394 (2020).
4. Socie, E., Vale, B. R. C., Burgos-Caminal, A. & Moser, J. E. Direct Observation of Shallow Trap States in Thermal Equilibrium with Band-Edge Excitons in Strongly Confined CsPbBr₃ Perovskite Nanoplatelets. *Adv. Opt. Mater.* **2001308**, 1–6 (2020).
5. Li, Q., Yang, Y., Que, W. & Lian, T. Size- and Morphology-Dependent Auger Recombination in CsPbBr₃ Perovskite Two-Dimensional Nanoplatelets and One-Dimensional Nanorods. *Nano Lett.* **19**, 5620–5627 (2019).